Q. J. R. Meteorol. Soc. (2005), **131**, pp. 1461–1482 doi: 10.1256/qj.03.189

Analysis of the African easterly jet, using aircraft observations from the JET2000 experiment

By DOUGLAS J. PARKER[1]*, CHRIS D. THORNCROFT[2], RALPH R. BURTON[1] and AÏDA DIONGUE-NIANG[3]

[1]*Institute for Atmospheric Science, University of Leeds, UK*
[2]*Dept of Earth and Atmospheric Sciences, University at Albany, SUNY, Albany NY, USA*
[3]*Direction de la Météorologie Nationale, Dakar-Yoff, Senegal*

(Received 5 September 2003; revised 29 September 2004)

SUMMARY

Analyses of the African easterly jet (AEJ) are presented which are based on meridional transects of high-resolution dropsonde observations made during JET2000, an aircraft campaign conducted in the last week of August 2000. The observations have confirmed that the AEJ is closely defined by geostrophic balance. The baroclinicity between the extreme northern and southern profiles accurately determines the altitude of the jet core, while the location and morphology of the jet core correspond to a locally-defined geostrophic wind measure. The potential-vorticity (PV) structure has also been found to accord with theoretical expectations, with distinctive positive- and negative-PV anomalies equatorward and poleward of the jet core respectively.

The thermodynamic structure of the AEJ environment can be categorized into coherent layers. The monsoon layer is a humid zone connected to the land surface, extending northwards into the Sahel and increasing in depth towards the south. This layer is affected by the land surface on diurnal time-scales, through the growing convective mixed layer and through shallow cumulus clouds. Above the monsoon layer is the Saharan air layer (SAL), which can be identified as a layer of low static-stability and low PV. The SAL is deep where it merges with the Saharan boundary-layer in the north, and becomes thinner toward the south. It has been shown that the boundaries of the SAL can be approximated to good accuracy as adiabatic surfaces, meaning that the SAL comprises air which is adiabatically connected to the land surface via the Saharan boundary-layer. The upper region of the SAL is identified as a layer of high relative-humidity where altocumulus and stratocumulus layers are observed. Finally, the troposphere above the SAL is again almost pseudoadiabatic, with small baroclinicity which determines the closure of the AEJ core aloft. Through inspection of thermodynamic tracers, evidence of convective and lateral transport and exchange between these layers is also presented.

KEYWORDS: African easterly waves Diurnal cycle Mesoscale convective system West African monsoon Sahel

1. INTRODUCTION

The African easterly jet (AEJ) is a midtropospheric jet located over tropical north Africa during the northern hemisphere summer (e.g. Burpee 1972). It is a key feature of the West African monsoon (WAM), linking large-scale aspects of the WAM to its characteristic weather systems. Its vertical shear is important for the growth of long-lived mesoscale convective systems (MCSs) (e.g. Houze and Betts 1981) and its potential-vorticity (PV) and low-level-temperature contrasts are important for African-easterly-wave (AEW) development (e.g. Burpee 1972; Thorncroft and Hoskins 1994). While it is well known that the AEJ arises in association with the large-scale low-level-temperature contrasts between the Sahara and the Guinea Coast, the multi-scale processes that act to determine the observed AEJ are not well understood. Through analysis of high-resolution observations made during the JET2000 aircraft campaign of the last week of August 2000 (Thorncroft *et al.* 2003; hereafter T03), the present paper explores the AEJ and considers the processes that influence it.

To a first approximation, the WAM can be viewed as an annually varying, zonally symmetric, and thermally direct circulation that is established in association with the large-scale meridional gradients in boundary-layer equivalent potential temperature (θ_e)

* Corresponding author: Institute for Atmospheric Science, School of the Environment, University of Leeds, Leeds, LS2 9JT, UK. e-mail: doug@env.leeds.ac.uk

between the continent and the Atlantic Ocean to the south (e.g. Eltahir and Gong 1996). The situation over the continent is complicated by the presence of marked meridional gradients in boundary-layer potential temperature (θ) between the Sahara and the Guinea coast, with highest θ polewards of the highest θ_e. Dry convection characterizes the high-θ region and is associated with a thermally direct heat-low circulation that fills the lower troposphere (Thorncroft and Blackburn 1999, hereafter TB).

TB discussed the role of convection in communicating the low-level θ and θ_e contrasts in the vertical, and the significance of this for the AEJ. Dry convection, expected to characterize the hot dry desert region, results in a vertical temperature-profile close to a dry adiabat. In contrast, deep moist convection, expected to characterize the cooler moist boundary-layer south of this, results in a vertical temperature-profile closer to a moist adiabat. The dry and moist adiabats are expected to meet and cross at mid-levels, as a consequence of the negative meridional gradients of θ_e at low levels, and this results in the observed midtropospheric easterly wind maximum around 600–700 hPa. The AEJ, viewed in these terms, forms through the action of surface fluxes and convection communicating the temperature contrasts vertically, and an adjustment of the atmosphere to thermal-wind balance.

As discussed by T03, the above description of the AEJ is based on simplistic assumptions about the thermodynamic profiles, and it is important to consider the extent to which the moist and dry convecting regions interact. In the upper part of the heat-low circulation we expect equatorward advection of dry air towards the moist convecting region, analogous to the dry intrusions in the tropical western Pacific (e.g. Parsons *et al.* 2000). This is likely to influence moist convection (suppressing shallow cumulus, but giving the potential for intense downdraughts in deep cumulonimbus systems) and to impact the mean thermodynamic profiles (cf. Robe and Emanuel 2001). At the same time, in the lower part of the heat-low circulation, we find poleward advection of moist air towards the dry convecting region. This is likely to enhance the probability of moist convection and cloud cover poleward of the main rainy zone in the high θ_e region and will also impact the mean thermodynamic profiles there.

An important characteristic of the AEJ expected to influence the AEW activity is the negative meridional gradient of PV at the core of the jet (e.g. Burpee 1972; Pytharoulis and Thorncroft 1999). As discussed by TB, this gradient can be understood in terms of the PV anomalies that are generated by the moist and dry convection. A positive PV-anomaly is generated beneath the diabatic heating maximum in the ITCZ (Schubert *et al.* 1991) and a negative PV-anomaly is generated in the heat low in association with the low static-stability. The sparsity of the routine observing network, particularly in the meridional direction (see T03) means that it is not possible to diagnose this key characteristic of the AEJ. High-resolution observations are required that resolve the PV contrasts.

The mean convection view proposed by TB is further complicated by the possible impact of organized mesoscale convective systems (MCSs) (e.g. Diongue *et al.* 2002; Redelsperger *et al.* 2002). Such systems may have a dynamical impact on the AEJ through the vertical and meridional transport of momentum (e.g. Moncrieff 1992; LeMone and Moncrieff 1994; Caniaux *et al.* 1995), as well as through modification of the thermodynamic profiles and consequent geostrophic adjustment. The extent to which the AEJ is accelerated or decelerated by these processes remains unclear. Parker and Burton (2002) have noted that a two-dimensional perspective of the impact of MCSs on the AEJ is inadequate. MCSs have limited meridional extent and induce significant meridional winds. Since the MCSs propagate along a strong baroclinic zone, their impact on the basic state AEJ and its synoptic variability depends on meridional

advective processes as well as the meridional variations in the PV structures generated by the MCS thermodynamic forcing.

From this discussion it is clear that the observed AEJ arises in association with processes acting on various space- and time-scales. It is therefore a serious challenge for GCMs used for weather- and climate-prediction to represent these processes realistically. Unfortunately, we are hindered in improving our understanding of the AEJ, and in assessing the ability of GCMs to represent it and these associated processes, by the sparsity of the routine observing network. This strongly motivated the JET2000 experiment, which used a C-130 aircraft to make high-resolution observations of the AEJ during the last week of August 2000, including transects along and across the AEJ (see T03). The dropsonde and aircraft observations give us a synoptic 'snapshot' of the AEJ of unprecedented resolution, allowing a detailed assessment of the AEJ structure and a consideration of the processes that influence it. Moreover, the observation that the experiment took place in a period of weak synoptic variability (T03) means that this snapshot is particularly representative of the 'basic state' AEJ.

The present paper aims to provide an objective analysis of the AEJ, including its dynamic and thermodynamic structure as observed during the JET2000 campaign. This, arguably, provides spatially the highest resolution view of the AEJ ever obtained, if only for a few days. The pattern of soundings from the dropsondes resolves significant features of the state of the atmosphere, including the structures of the AEJ, baroclinic layer, monsoon layer and Saharan layer, at a horizontal resolution of about half a degree of latitude.

The flight paths and methods of synthesizing the data are briefly described in section 2, while section 3 describes the wider synoptic situation in which the dropsonde 'snapshots' are embedded. Section 4 presents and discusses the observations, including a consideration of the thermodynamic and dynamic structure of the AEJ and the relationship with the boundary-layer θ and θ_e gradients. Section 5 presents and discusses the generality of these conclusions, using dropsonde sections from the other meridional flight-legs. The paper concludes with a discussion section.

2. Experimental details and synthesis of the data

The flight details are only briefly described here: for more details of the logistics, refer to T03. The C-130 undertook two north–south oriented box flights on 28 and 29 August 2000. These flights (referred to as flight 2 and flight 3) started and finished in Niamey, Niger, and each flight included two long north–south legs, at longitudes 1.7°E and 2.2°E, across the AEJ. During each flight, dropsondes were released at approximately 50 km (0.5 degrees of latitude) intervals on the eastern leg and 100 km (1 degree) intervals on the western leg. On each of flights 2 and 3, a low-level flight was conducted at 877 hPa, along the track of the eastern leg: for flight 2, this low-level section extended between 9.8°N and 16.5°N. The majority of the discussion in the paper is based around the high-resolution eastern leg of flight 2, at 2.2°E, shown by a heavy line on Fig. 1.

The quality of the dropsonde data from the experiment is generally excellent, although there is some loss of wind data from low levels. Two methods of synthesizing the data from the set of dropsondes have been employed. The first uses linear interpolation in the vertical, onto a 2 hPa grid in pressure, which has the advantage of being exact at the data sampling points. Where data are missing from a single profile, horizontal linear interpolation from adjacent good data is used. This method is preferred for the consideration of fine structure, in the majority of the figures presented here, but when

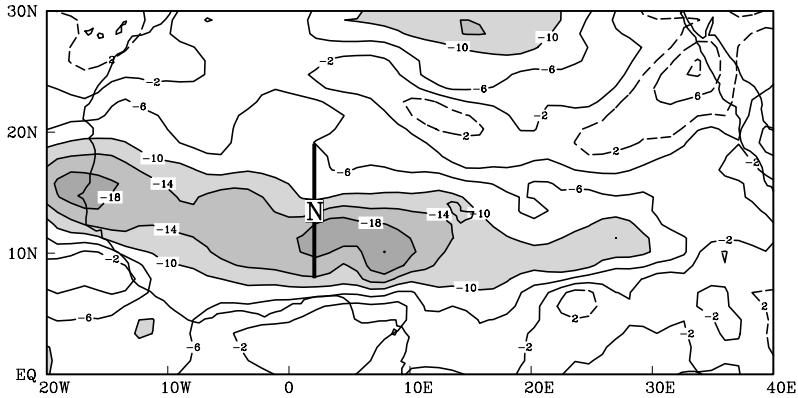

Figure 1. Zonal wind u from ECMWF's operational analysis fields at 700 hPa for 1200 UTC, 28 August 2000, contoured at 4 m s^{-1} intervals, with easterlies stronger than 10 m s^{-1} shaded. The eastern leg of flight 2 is indicated by a bold line, along 2.2°E, with the location of Niamey, Niger, indicated by the boxed letter N.

diagnostics involving vertical derivatives (of winds in particular) are being computed, significant smoothing is often needed. For this reason, the successive correction method (SCM) has been employed to approximate the raw data on the regular grid in the computation of PV (see Pedder 1993 or Daley 1995).

3. Synoptic overview

For reference, and for an appreciation of the large-scale synoptic situation, we briefly describe the analysis by the European Centre for Medium-Range Weather Forecasts (ECMWF) of the winds at 700 hPa for 1200 UTC, 28 August 2000 (Fig. 1). While considering these, it should be realized that many of the dropsondes released from the aircraft were included in these operational analyses. The AEJ is seen as a prominent feature with easterlies present over much of tropical north Africa and an AEJ axis equatorward of Niamey around 10–14°N. Equatorwards and east of Niamey, the AEJ peak values are greater than 20 m s^{-1}—much larger than those often quoted for the mean AEJ (Burpee 1972; Reed *et al.* 1977). As discussed by T03, the AEW structures at the latitude of the AEJ were weak during the period of the flights. In the present paper, we capitalize on the weak synoptic variability to make statements about the undisturbed AEJ.

Taylor *et al.* (2003) discussed convective storms which crossed the flight paths during the 24 hours before flight 2. There appear to have been two principal bands of rainfall, one between 14°N and 16.5°N and another south of 12°N, occurring after an unusually dry spell for the northern Sahel. From the observations of Taylor *et al.* (2003), we conclude that the resulting land-surface-moisture patterns were communicated efficiently and rapidly into the local convective mixed layer (hereafter ML): clarifying how this thermodynamic structure is related to the dynamics of the AEJ is the purpose of the present paper.

4. Observations of the AEJ

The *observed* structure of the AEJ will be described in this section, based on the high-resolution eastern leg of flight 2 made on 28 August 2000. At this point it must be made clear that the near-synoptic observations described here are not intended to make

a direct test of previous climatic analyses, such as those of Burpee (1972). With these present observational analyses, we aim to test physical models of the AEJ structure and evolution, with which to develop our physical interpretation of such climatological data. Furthermore, the fact that the period of these flights was one of weak synoptic activity enables us to interpret the observations as representing the basic undisturbed state with more confidence.

(*a*) *Basic jet structure on 28 August 2000*

Distributions of zonal wind u and virtual potential temperature θ_v are shown in Figs. 2(a) and 2(b). In a broad sense, the AEJ structure is similar to those seen in previous observational studies (e.g. Burpee 1972; Reed *et al.* 1977). It has a well-defined jet core, located around 650 hPa and 10°N, an associated markedly baroclinic zone beneath this (sloping downwards to the north) and weaker, reversed, baroclinicity above. The core of the jet is well captured and indicates peak easterly winds of 21.3 m s^{-1} that are much stronger than the climatological average. The jet is also located south of its climatological position for August. Together, these abnormalities may be consistent with the dry spell that characterized the region during the JET2000 experiment (Newell and Kidson 1984; T03; Matthews 2004).

The jet weakens with latitude as expected, but there are also significant changes in the shear profiles. Marked vertical shear characterizes the lower troposphere beneath the jet core. Polewards of this, the peak shears tend to follow the downward sloping baroclinic zone. Above this baroclinic zone and polewards of the jet core, the vertical shear of the zonal wind is noticeably weak, consistent with the weaker baroclinicity there. It is also consistent with vertical mixing of momentum. It is intriguing to note that this region of low vertical wind-shear is also a region of relatively low static-stability as indicated by the θ_v distribution. This region would not be able to support strong vertical shears since the Richardson number would then become low, allowing shear-driven instability to develop. Significantly for the organization of cumulonimbus systems, there is easterly vertical shear of the zonal wind in the lower troposphere, up to around 800 hPa, in all the profiles between 8°N and 19°N.

A closer look at the θ_v distribution (Fig. 2(b)), and the patterns of Brunt–Väisälä frequency (Fig. 2(c)), reveals the considerable vertical and meridional variations in stability that characterize the AEJ region. The neutrally-stratified dry convective ML at low-levels (diagnosed as a layer of small parcel-buoyancy anomalies, and plotted as a bold dashed contour) extends up to about 950 hPa south of 16°N but becomes much deeper north of this latitude. Polewards of about 16.5°N, on the fringes of the Sahara, the atmosphere is characterized by very low static-stability, almost uniformly from the surface up to around 600 hPa. In the northernmost profiles, the residual Saharan boundary-layer from the previous day reaches 600 hPa, and there is an internal ML growing into this (up to a level of 850 hPa at 19°N at 1110 UTC). Equatorwards of about 16.5°N, the structure of the atmosphere is dominated by the sloping baroclinic zone that lies above the ML. Above the baroclinic zone, the atmosphere exhibits low static-stability, even detectable as far south as 8°N: this is an example of an 'elevated mixed layer' as described by Carlson (1998, chapter 16). Owing to the north–south continuity in the near-neutral layer above the baroclinic zone, and the fact that isentropes in the layer are connected to the Saharan boundary-layer, there is a strong indication that some of the air in this layer originated over the Sahara. This layer is sometimes referred to as the Saharan air layer (SAL) (e.g. Karyampudi *et al.* 1999) and is characterized by high aerosol-dust content, consistent with low visibility on the flight. Here, we use the term SAL to describe this layer of low stability, but recognize that this is not necessarily

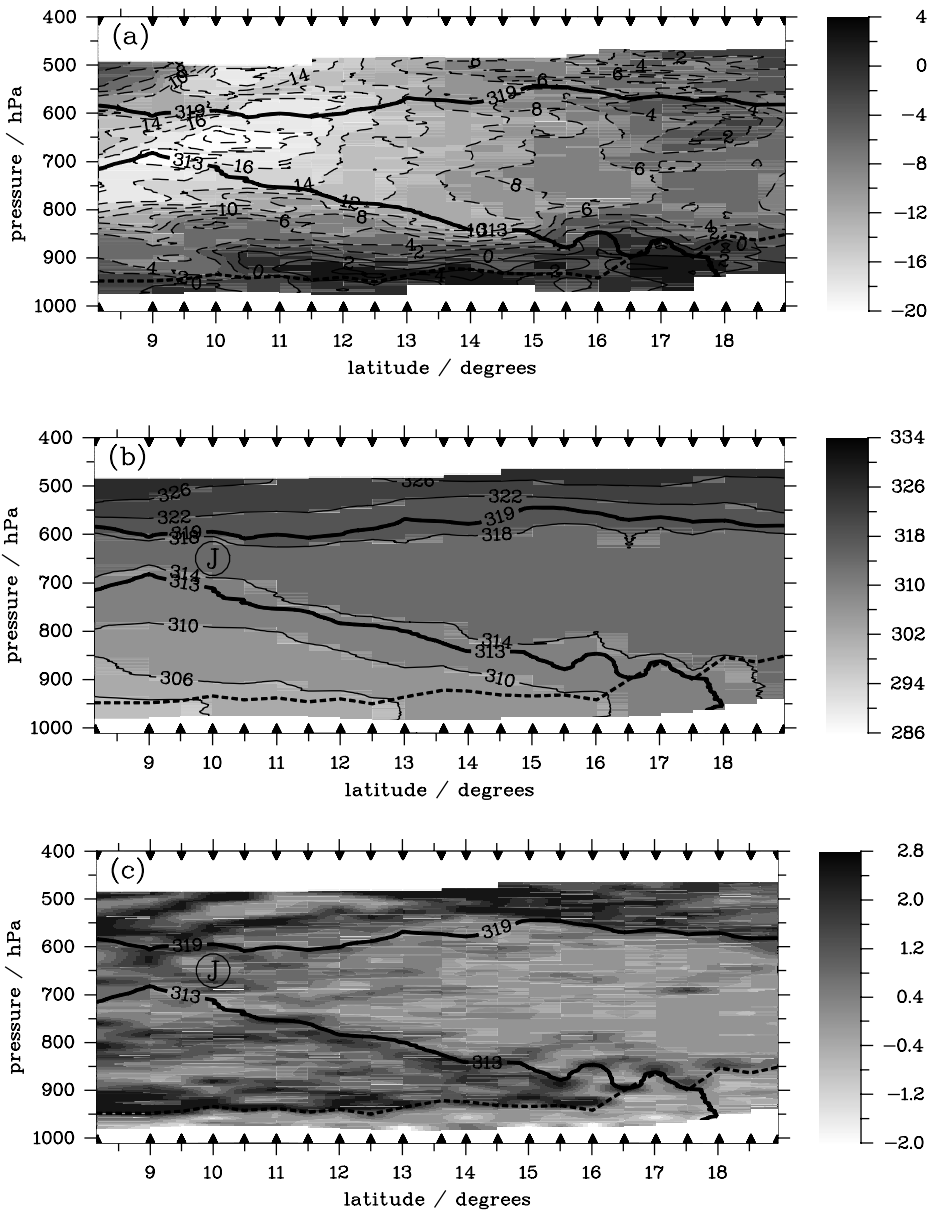

Figure 2. Latitude–pressure sections derived from the set of sondes dropped on the eastern leg of flight 2, on 28 August 2000: (a) zonal wind u (contoured at 2 m s^{-1} intervals); (b) virtual potential temperature (contoured at 4 K intervals) and (c) squared Brunt–Väisälä frequency N^2 (units of 10^{-4} s^{-2}). Negative contours are dashed. Black triangles at the upper and lower boundaries denote the dropsonde positions. Bold contours of $\theta_v = 313$ K and $\theta_v = 319$ K are superposed, as measures of the 'Saharan Air Layer' extent. The top of the mixed layer (deduced from parcel buoyancy) is marked by a thick dashed curve, and the position of the core of the African easterly jet by an encircled J.

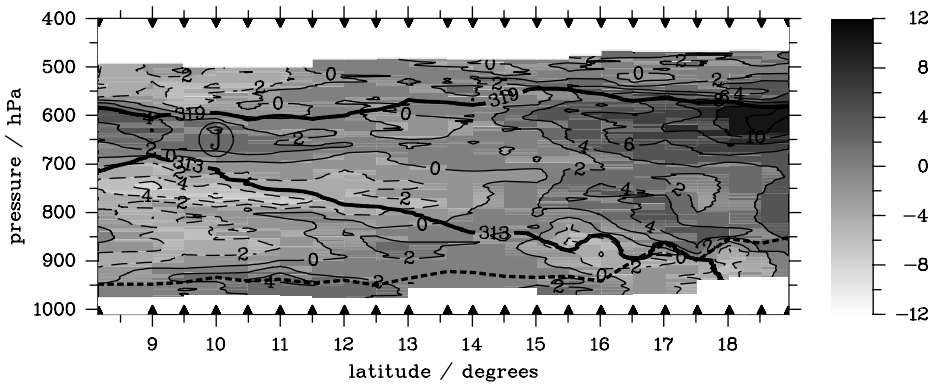

Figure 3. As Fig. 2(a), but for meridional wind v (contoured at 2 m s^{-1} intervals).

a layer whose composition is uniquely derived from the Saharan boundary-layer: it is also possible for air to move into this region out of the rainy zone through adiabatic motion. In subsection 4(c), evidence is presented of this kind of lateral exchange along isentropes that link the Saharan surface with the ITCZ.

Based on this analysis, it appears that the SAL can be reasonably well defined by the low-stability region and, furthermore, that this region is approximately bounded by the $\theta_v = 313$ K and $\theta_v = 319$ K contours (marked in bold in Fig. 2(b)). Using this definition, we see the base of the SAL rise above the surface south of about 16.5°N and reach nearly 700 hPa towards the south of the transect, while the top of the SAL is more constant at around 550–600 hPa. The SAL becomes far less well defined in the southernmost profiles, and from the stability plot (Fig. 2(c)), we see that, in this case, the adiabatic limits should probably only be used down to a southerly latitude of around 10 or 11°N. The choice of these two particular adiabats to define the upper and lower limits of the SAL works well for all four meridional flight legs conducted over two days in August 2000; further support for this method of characterizing the layers appears in the analysis of moisture variables in subsection 4(c).

We would emphasize that our use of adiabatic surfaces to define the bounds of the monsoon layer and SAL is empirical, and that we have subjectively chosen values of θ_v which define these bounds in the data shown here. The use of adiabatic surfaces can be justified by noting that the SAL is close to constant θ_v and that its bounding layers above and below are more stable. If we choose an adiabat within the stable transition between the layers, the errors in the resulting height estimate will be small. We also recognize that the absolute values of these surfaces may vary with longitude and time (as may be inferred from the model results of Karyampudi and Carlson (1988)).

These adiabatic boundaries now highlight the different layers that characterize the baroclinic region: (i) the monsoon layer capped by the base of the SAL, (ii) the SAL itself and (iii) the troposphere above the SAL. In addition to these three characteristic layers, a diurnally varying convective ML grows upwards during the day, into the monsoon layer in the south and into the Saharan residual layer in the north. The adiabatic SAL boundaries are included in subsequent plots for reference.

In a given profile, operational forecasters typically define the top of the monsoon layer as being the level at which $v = 0$, and this height is used as a primary measure of the likelihood of subsequent moist convection (e.g. Eldridge 1957).

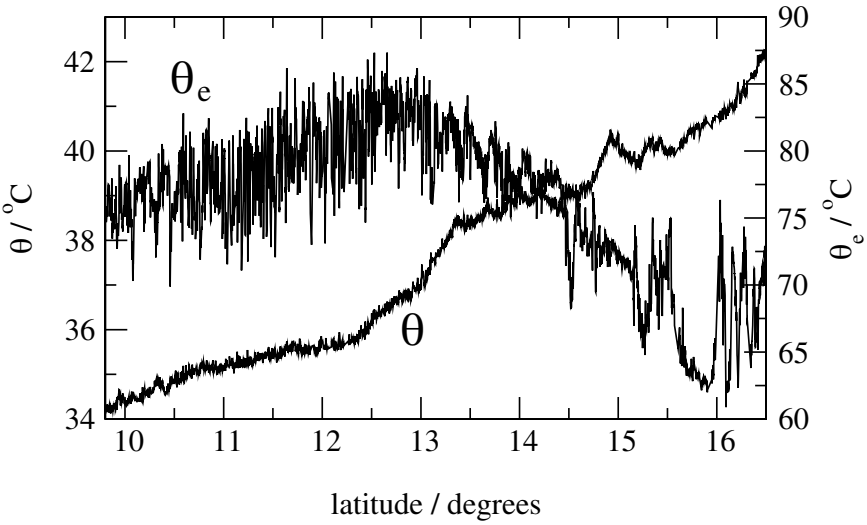

Figure 4. Potential temperature θ and equivalent potential temperature θ_e (both °C) at low levels, plotted as a function of latitude, from the boundary-layer flight conducted at the 877 hPa level on 28 August 2000.

However, from Fig. 3 it can be seen that the contour of $v = 0$ is highly variable, does not correspond well to the base of the SAL and is therefore not a good measure of monsoon-layer depth.

(*b*) *Thermodynamic profiles and thermal-wind balance*

(i) *Thermodynamic profiles.* TB argued that the observed mid-level zonal wind maximum arises because the AEJ is in thermal-wind balance with the temperature structure in the troposphere that is established in association with deep moist convection in the ITCZ and dry convection in the lower troposphere in the Sahara. The tropospheric temperatures are assumed to be a reflection of the low-level θ_e in the ITCZ region and the low-level θ in the Saharan region. Figure 4 shows the θ and θ_e from the low-level flight which was made approximately 4.5 hours after the dropsonde flight at the same longitude. The broad features of this plot are an increase in θ towards the north, and a θ_e maximum at a latitude of 12–13°N: note that the AEJ maximum lies to the south of the θ_e peak in this synoptic section. Taylor *et al.* (2003) have made a detailed discussion of the fine-scale variations in the low-level properties on these flights: in particular, regions of strong gradients of θ, at 12.5–13.5°N and 15.5–16.5°N, both appear to be a result of recent rainfall to the southern side of these zones and are directly linked to the local surface.

Figures 5(a) and 5(c) show tephigrams from 8°N and 19°N, the meridional extremes of this section*. The temperature profile at 19°N (Fig. 5(c)) is dominated by a deep, dry adiabatic layer between 625 hPa and 850 hPa, with a new layer developing beneath. In contrast, the profile at 8°N (Fig. 5(a)) is closer to pseudoadiabatic, with higher humidities. The result is that the two temperature profiles cross at around 625 hPa close to the observed AEJ height in Fig. 2(a), confirming, in this instance, the conceptual model of TB. However, the observed AEJ will be influenced by the thermodynamic

* Note: comparison of Figs. 4 and 5 shows the diurnal warming at low levels in the interval between the boundary-layer flight and the earlier dropsonde flight that day, 28 August.

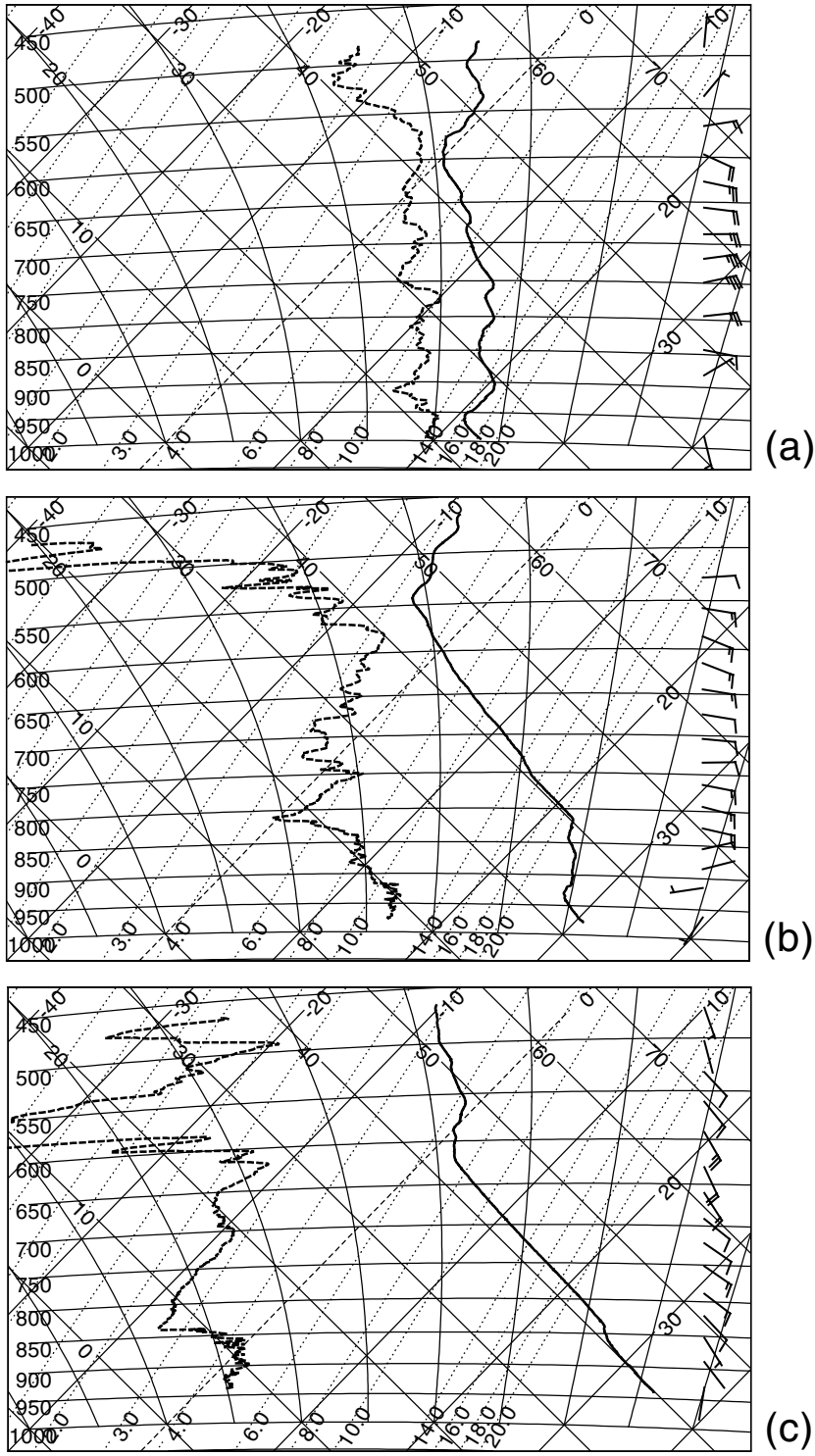

Figure 5. Tephigrams using data from sondes dropped during flight 2, on 28 August 2000: (a) 8°N; (b) 15°N and (c) 19°N. The monsoon layer (at heights below 815 hPa), 'Saharan Air Layer' (815–545 hPa) and upper tropospheric layer (above the 545 hPa level) are evident in panel (b).

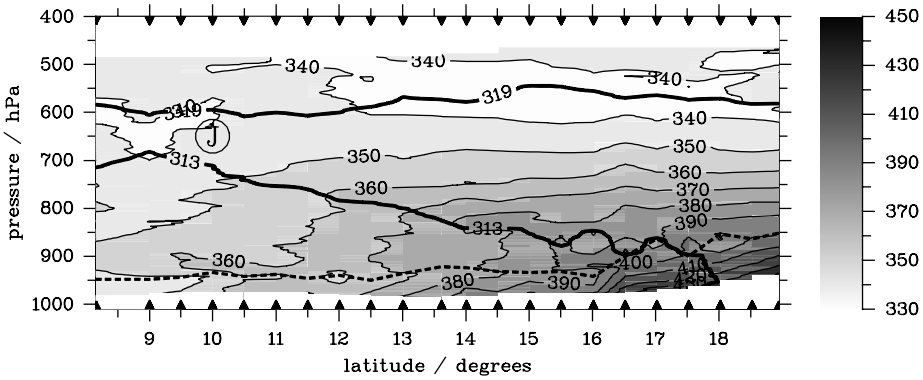

Figure 6. As Fig. 2(b), but for saturated equivalent-potential-temperature θ_{es}, contoured at 10 K intervals.

conditions across the whole region, not just at the extremes. We will consider these variations by examining the saturated equivalent-potential-temperature (θ_{es}) structure of the AEJ (Fig. 6). In regions characterized by moist convection, θ_{es} tends to be nearly constant with height, implying a vertical profile close to a moist adiabat. In contrast, regions characterized by dry adiabats in association with dry convecting boundary layers will have strong vertical gradients of θ_{es}. Again we see this clearly at the poleward extremes.

The region between the two extreme latitudes is more complicated and has characteristics of both regions. The layered structure that characterizes the baroclinic zone is exemplified by the tephigram at 15°N (Fig. 5(b)). As noticed earlier, the monsoon layer has a developing ML up to about 940 hPa at this time. Above this, the monsoon layer has a vertical temperature profile which is nearly pseudoadiabatic, consistent with its being strongly influenced by cumulus convection (up to 815 hPa in Fig. 5(b)). Note that the value of θ_{es} in the monsoon layer is here (and typically) greater than the θ_e of the mixed-layer: in this region of strong diurnal cycle in surface fluxes, and strong convective inhibition, there is not a local and instantaneous equilibrium between the boundary-layer θ_e and the pseudoadiabatic profile above it. The SAL above this is characterized by strong vertical gradients in θ_{es} (Fig. 6), consistent with the temperature profiles being close to a dry adiabat (Fig. 5(b)). We note that while the monsoon layer is impacted by moist convection that communicates the low-level θ_e up to the base of the SAL, the SAL has weak thermodynamic connection with the surface below and is more closely linked to the Saharan region. The SAL is clearly capped by an inversion, at a level of around 540 hPa at 15°N (Fig. 5(b)).

Returning to Fig. 6, the troposphere above the SAL is only weakly baroclinic, and is close to pseudoadiabatic in the south of the section (at least in the range of pressure levels available here), suggesting adjustment to a moist convecting regime. Towards the north, the air immediately above the SAL is more stable. Small horizontal gradients in θ_{es} at this level (compare the upper values at 8°N and 19°N in Fig. 2(b), for example) appear to be important to the balance in the jet, since they determine the reversal of the zonal shear above the AEJ, as manifested in the thermal-wind estimates computed in the next subsection.

(ii) *Thermal-wind balance.* From the previous subsection we can hypothesize that the observed tropospheric temperature in the vicinity of the AEJ is influenced by a combination of processes. It arises in association with deep moist convection in the

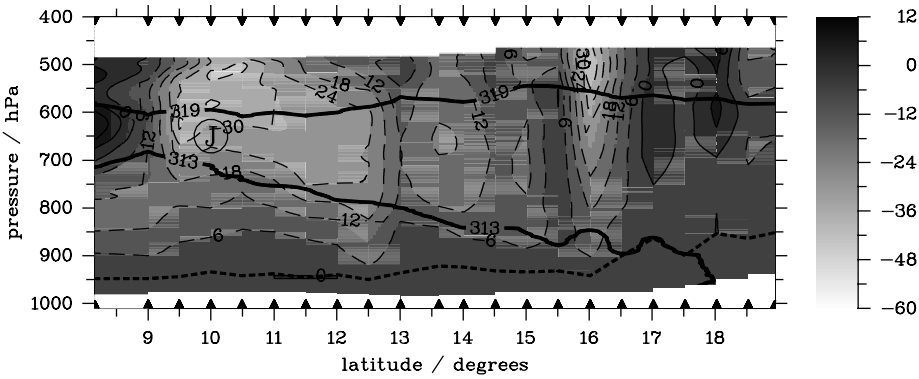

Figure 7. As Fig. 2(b) but for the bulk geostrophic zonal wind shear, as estimated from the thermal-wind equation (contoured at 6 m s^{-1} intervals; see text for details).

south, deep dry convection in the north, and shallow moist convection between them that is capped by the SAL aloft. Given this, it is important to assess the extent to which this temperature structure is important for the AEJ and the extent to which the AEJ is in balance with this temperature structure.

The geostrophic wind shear has here been derived from the thermal-wind equation, which is an exact diagnostic relation. For simplicity, we estimate a local value of geostrophic zonal wind component, Δu_g, by taking a reference value of geostrophic wind, $u_g = 0$, at the top of the convective ML and integrating upwards (Fig. 7). Comparing these winds and their associated shears with the observed winds in Fig. 2(a) allows an assessment to be made of the extent to which the AEJ is in thermal-wind balance. It can be seen that the main structural features of the AEJ are picked up by the geostrophic wind, notably its peak latitude. Although the extremum in Δu_g is around 50 hPa higher in elevation than the level of the AEJ core, the double maximum in the jet at 10°N, and the downward slope of the jet maximum to the north over 10–12.5°N are reproduced by Δu_g.

The geostrophic wind shear in the AEJ is generally larger than the observed wind shear by about 50%: it is interesting to compare this with the results of Cook (1999), who found only small ageostrophic zonal winds (as opposed to shear) in the mean AEJ of an NCEP climatology. In terms of the meridional momentum balance, the easterly ageostrophic wind-shear with height in our observations is consistent with the presence of turbulent friction in the layer below the AEJ or with meridional acceleration.

Between 16°N and 18°N, there are strong fluctuations in estimated geostrophic wind, which have no obvious relationship to observed zonal winds. Inspection of the θ_v pattern (and θ_{es}) shows that the fluctuations in geostrophic wind are related to small-scale, apparently unbalanced, thermal fluctuations on the scale of the dropsonde spacing. Such thermal features may arise through the low stability of the SAL in this region, which will allow significant vertical motion to develop. This region, being the baroclinic transition from the relatively stable monsoon layer to the convective Saharan boundary-layer, is likely to be a zone which is dynamically active near the surface, and therefore forcing gravity waves in the layer above. Without more detailed observations or modelling we cannot determine the cause of these local buoyancy fluctuations exactly, but we indicate this region as interesting for further study.

(iii) *Potential vorticity.* The fact that the AEJ is close to thermal-wind balance at this time supports the use of diagnostics that make use of balanced concepts, including PV.

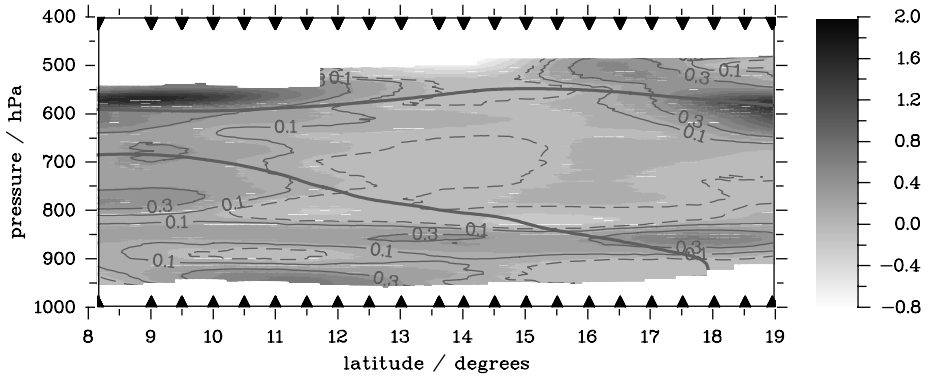

Figure 8. As Fig. 2(b) but for potential vorticity (1 PVU $= 10^{-6}$ K m^{2}kg^{-1}s^{-1}). Solid contours of 0.1 and 0.3 PVU are shown, and the zero contour is dashed (see text for details).

Our knowledge of the observed PV structure of the AEJ is limited: estimates suffer from poor resolution in the meridional direction, especially north of 13.5N. As a result, the PV diagnosed by Burpee (1972) did not indicate the expected significantly negative PV-anomaly associated with the deep Saharan boundary-layer. It should be noted that operational analyses also suffer from this gap in radiosonde observations and so, to represent the state of the atmosphere in this area, rely heavily on streams of other observational data whose value is less well understood, and on model internal processes.

The PV structure presented in Fig. 8 is estimated using information from both the eastern and western legs of the flight. The full Ertel PV is estimated but without terms involving the vertical velocity since we do not have sufficiently accurate observations of this field. We have also taken no account of the time-lag between observations made on the eastern and western legs.

Consistent with TB, we see that the AEJ is associated with two distinctive PV features. A negative PV-anomaly and associated low static-stability is established in the dry convecting region on the poleward side of the AEJ. The present observations show that this negative PV anomaly also characterizes the SAL, consistent with low stability and the likely Saharan origin of air in this layer. As expected, there is also a prominent positive PV anomaly on the equatorward side of the AEJ. This is consistent with the cyclonic shear and, as proposed by TB and Schubert *et al.* (1991), is likely to be produced in association with deep moist convection just equatorwards of this. It is the proximity of these two diabatically generated PV-anomalies, combined with the low-level temperature gradients, that provides the necessary conditions for mixed barotropic–baroclinic instability of the AEJ.

The AEJ is influenced by other PV anomalies in addition to these. Positive PV-anomalies characterize the stable layers at the upper and lower limits of the SAL. Complex PV structures characterize the air in the monsoon layer, where PV is influenced by a combination of processes including advection from low and southern latitudes, as well as local modification through diabatic processes, the details of which are beyond the scope of this analysis. The temporal development of the ML at low levels, with a shallow stable layer between the ML and the Saharan residual layer, also leads to apparent PV anomalies in the north, e.g. at 875 hPa, 18°N. However, as already mentioned, the interval between the flight-legs makes values of the PV calculated in the ML unreliable.

By showing the PV structure of the AEJ in this synoptic set of data, we have confirmed the ideas of simple models of AEJ stability and have shown the SAL to consist

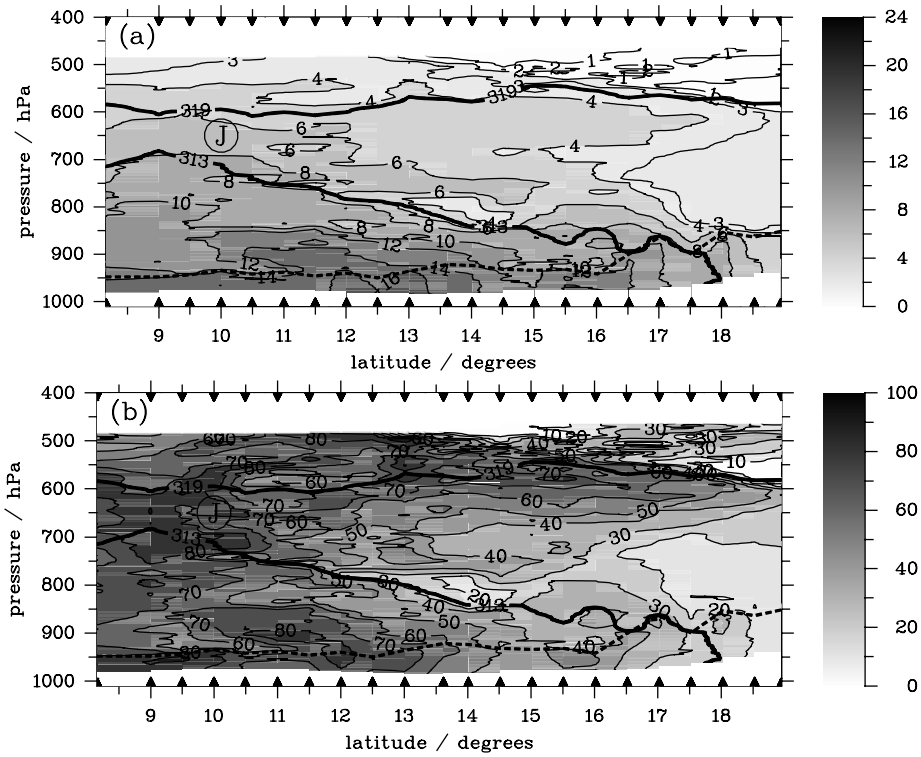

Figure 9. As Fig. 2(b) but showing (a) humidity mixing ratio r (contoured at 1 g kg^{-1} intervals for $r \leq 4$ g kg^{-1} and at 2 g kg^{-1} intervals otherwise) and (b) relative humidity (contoured at 10% intervals).

of air with low PV, consistent with its Saharan origin. The PV patterns shown here may also represent a target for GCMs, which need to resolve the PV structure in order to correctly represent AEW development through instability mechanisms.

(*c*) *Humidity structure and convection*

(i) *Humidity profiles.* Figure 9 shows the humidity mixing ratio, r, and relative humidity, RH, together with the adiabatic boundaries of the SAL. The monsoon layer beneath the SAL exhibits relatively high r of 14 g kg^{-1} and greater, with maximum values around 12–13°N. The SAL above this is characterized by much smaller values. Finally, the troposphere above the SAL shows extremely small r, with values in the north measured as less than 0.02 g kg^{-1} (below the dropsonde accuracy of around 2% RH), consistent with large-scale subsidence. A closer look at these observations shows fine structure within all the layers, which is coherent over several dropsondes, and indicates that the adiabatically-defined layers are complicated by the interplay between lateral advection and convective transport or mixing of water vapour.

As with the earlier discussions of thermodynamic structure it is convenient to start with the two extreme latitudes. The poleward region consists of a deep residual boundary-layer characterized by very low values of $r < 3$ g kg^{-1}, and a growing ML beneath with slightly higher r. The higher moisture content of the ML in the northern profile is consistent with an encroachment of moisture from the south in association with diurnally varying heat low circulations (Rácz and Smith 1999), and with the process of

evaporation from the surface overnight. In contrast, the equatorward region consists of much higher values of r (with maximum $r \approx 14$ g kg^{-1}) throughout the lower troposphere. Here RH is close to 80% throughout the depth and θ_e is fairly uniform with height (with value around 337 K; not shown), consistent with a region that often experiences moist convection.

The humidity budget of the SAL has particular importance for several reasons. Dry air with low θ_e at mid-levels is needed for the formation of intense downdraughts, crucial for the establishment of long-lived MCSs. Since the SAL is associated with isentropes that connect the deep moist convecting zone to the Sahara, we expect horizontal moisture transport in this layer between the two regions. If dry air intrudes into the main rainy zone further south, we may expect this to impact the nature of convection there (see also Parsons *et al.* 2000). Inversely, moist air may be advected polewards towards the desert, where it may be entrained by the Saharan convective boundary-layer (CBL) during the day. The process of horizontal exchange may either occur at the mesoscale through detrainment in the anvils of cumulus clouds, or at the synoptic scale, through advection in association with the passage of AEWs. Such lateral exchanges are suggested by Fig. 9(a). At the base of the SAL we can see a dry intrusion extending between 10°N and 15°N whereas just above this there is evidence of a relatively moist layer whose origin may be further south. Similar layering in the SAL composition may be inferred in the thermodynamic profiles and lidar-derived dust measurements of Karyampudi *et al.* (1999).

A significant layer of high RH occurs at the top of the SAL: since the SAL is rather well mixed, and connected adiabatically to the well-mixed Saharan boundary-layer, it is natural for RH to increase with height in the layer. Above the SAL, the troposphere is generally very dry but RH increases towards the south of the domain and, except in the northernmost profiles, RH does not change abruptly at the top of the SAL. In the extreme southern profiles, the RH profile is comparatively uniform with height in this domain. In the field of mixing ratio (Fig. 9(a)) around 10.5–12°N and 550–600 hPa, there is evidence of horizontal moisture exchange at the top of the SAL, with an interleaving of humidity associated with local wind shear (Fig. 3).

As an example of the impact of convective penetration on the humidity structure of the layers, the MCS that occurred around 14–16°N on the previous day has locally impacted the moisture profile in the vertical. Low values of humidity and θ_e (not shown) at low levels are consistent with the redistribution of moisture by evaporatively driven downdraughts. A wedge of humid air can also be seen to protrude northwards, with its peak around 600 hPa, the level of maximum southerly winds. In these near-synoptic data, it is not easy to attribute this humidity structure to the different effects of mean-state, synoptically varying and convectively forced structures, but we must accept that the humidity structure observed is likely to contain a significant signal from the recent convective event. More evidence of MCS impacts on the layers was apparent on flight 3 (discussed briefly in T03).

(ii) *Clouds associated with the thermodynamic structure.* During the flights, we were able to make visual observations of the cloud fields, and, with the benefit of the thermodynamic data, these can be related rather clearly to the local stability and humidity patterns.

The monsoon layer, above the ML, was characterized by intermittent cumulus (humilis and congestus), with much horizontal variability (perhaps due to local surface moisture anomalies, as indicated by Taylor *et al.* (2003)) and a general tendency for a greater depth and density of cloud towards the south. As discussed in section 4.1,

the field of θ_{es} (Fig. 6) shows that the monsoon-layer profiles are, broadly speaking, close to a pseudoadiabat. Physically, then, we can regard the monsoon layer as a layer that is penetrated by shallow cumulus, since its profile is approximately neutral to this form of convective cloud instability. In this sense, we can regard the monsoon layer as being that layer which is controlled by an equilibrium with moist convection on intra-diurnal time-scales. Although the ML at the time of these dropsondes is shallow, we can expect convective clouds to develop within the monsoon layer, and to control its profile during the day.

A second characteristic layer of cumulus clouds was observed at the upper limits of the SAL, consisting of altocumulus and stratocumulus in the region of high relative humidity (Figs. 5(b,c) and 9(b)) at the top of the near-adiabatic part of the profile. On 28 August the northern extent of this cloud was around 13°N but on the following day altocumulus was observed at 18°N, at the top of a SAL which was more humid than that of 28 August. Recall that at this latitude, although the profile was nearly adiabatic, it consisted of a relatively shallow ML, and the clouds occurred at the top of a deeper residual layer. This kind of cloud layer has also been mentioned by Carlson (1998, chapter 16). Altostratus, cirrus and cirrocumulus were observed above the aircraft (and therefore above the SAL) during the high-level flights, at all latitudes.

To the south of the observational sections, deep cumulonimbus systems were seen. In addition to the deep convection observed visually, and the effects of MCS passages known to have occurred the previous day, cumulus penetration of the SAL was also observed. During flight 3 on 29 August 2000 (not shown) the aircraft flew over a cumulus top at 15°N and 500 hPa and a dropsonde released at this point observed the relatively humid column below. Given the neutrality of the SAL, cumulus detrainment is expected to be of greatest significance at the top of this layer (Bretherton and Smolarkiewicz 1989; Raymond and Blyth 1992), and this region is seen to have high relative humidity (Fig. 9(b)) and intermittent altocumulus.

5. Zonal and temporal variations

On the western leg of flight 2, sondes were dropped at intervals of one degree of latitude, over the same latitude range as on the eastern leg. The structures of the thermodynamic and wind fields from the eastern and western legs of this flight (not shown), which were separated by 0.5 degrees of longitude, are the same, and the main conclusions of the previous section regarding the state of balance of the jet and the characteristic layers (and their interactions) are robust. There is rather striking coincidence of small-scale features between the two legs, for instance the dry and more humid layers around 12–15°N, 850–700 hPa, in Fig. 9(a). Key differences between the fields in the two legs are all within the boundary layer and are fully consistent with the growth of the ML in the time interval (up to 2.5 hours) between the sets of observations. Such changes are then consistent with the diurnally-varying character of the monsoon layer which was proposed in the previous section, in contrast to the more slowly, or intermittently, varying behaviour in higher layers.

The observations made on flight legs the following day (29 August) showed some striking effects of deep convection (seen in Fig. 11 of T03), and some synoptic differences in the overall wind and thermodynamic patterns. However, the thermodynamic and dynamic patterns inferred on the basis of the 28 August 2000 flight (such as the monsoon layer and SAL characteristics) were found to be robust.

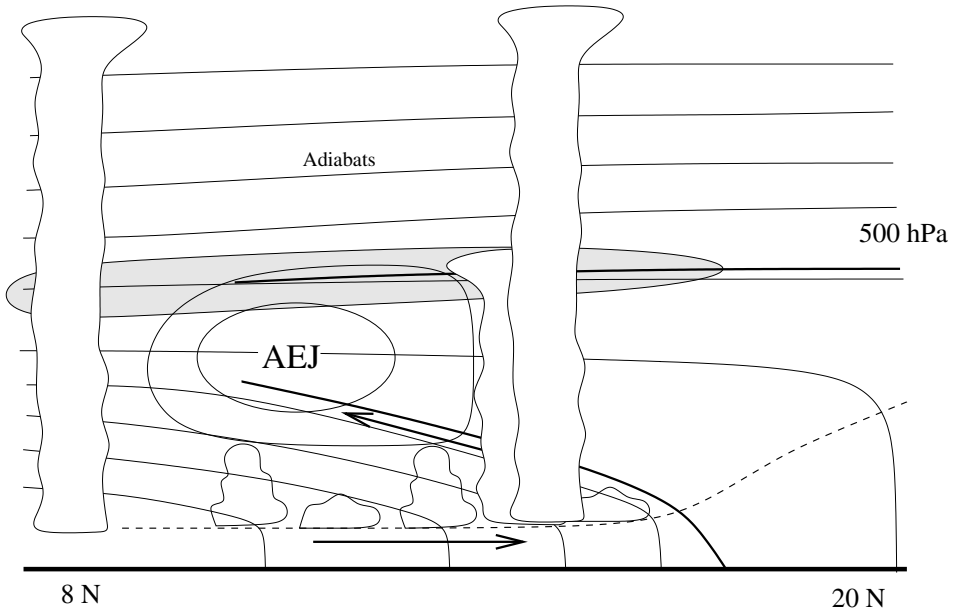

Figure 10. A schematic diagram of the thermodynamic structure on a latitude–height section through the African easterly jet system. Adiabatic 'Saharan Air Layer' (SAL) boundaries are denoted by bold lines and the top of the monsoon layer by a dashed line. A shallow layer of intermittent altocumulus and stratocumulus (grey shading) occurs at the top of the SAL, with increasing amounts and depth towards the south. The meridional circulation marked is that of the 28 August 2000 observations, and is expected to vary diurnally and synoptically.

6. Discussion and conclusions

Dropsonde data and aircraft observations made during the JET2000 experiment have been used to provide an analysis of the AEJ structure of unprecedented meridional resolution. On 28 August 2000, a fairly zonal jet with little impact of synoptic or mesoscale weather systems allowed us a view of a relatively undisturbed AEJ.

A schematic of the AEJ, based on the analysis of dropsonde and aircraft observations made on 28 August 2000 and on our current knowledge of the AEJ dynamics, is presented in Fig. 10. This schematic highlights the meridional variations in the structure of the AEJ including the variations in thermodynamic profiles that, through thermal-wind balance, define the AEJ winds. Following TB, we have confirmed the presence of two distinct convective regimes at the poleward and equatorward extremes of the region. The poleward region in the Sahara is characterized by a thermodynamic profile close to a dry adiabat, and consistent with the action of dry convection. The equatorward region has a thermodynamic profile that is closer to a pseudoadiabat, consistent with a strong influence of deep moist convection. In a bulk sense, the presence of the mid-level wind maximum around 650 hPa is consistent with thermal-wind balance and the fact that the meridional temperature contrast between these two profiles vanishes at that level.

In addition, our analysis has highlighted the structure of the baroclinic zone between these two extremes. The baroclinic zone is characterized by the presence of distinct layers: the monsoon layer at low-levels, the SAL overlying this and the troposphere above the SAL. These zones are distinguishable by their stability profiles, whether close to a dry or a moist adiabatic curve; furthermore, our analysis indicates that isentropic surfaces can be helpful when locating the vertical extent of the monsoon layer and the SAL (included as bold lines in the schematic). The observational sections also highlight

the presence of a diurnally varying ML that is shallow in the monsoon layer and rises steeply in the SAL.

The monsoon layer is characterized by a diurnally varying ML that is relatively moist, in association with surface fluxes and poleward advection. The profile above the ML is close to a pseudoadiabat, and therefore can be anticipated to support, and be in equilibrium with, shallow cumulus and stratocumulus, up to the level of the base of the SAL (which, being very dry, will tend to restrict shallow cumulus penetration (see Parsons *et al.* (2000))). There is a significant diurnal cycle in the structure of these clouds and of the convective ML. At the interface between the monsoon layer and the SAL, entrainment of dry SAL air into the monsoon layer may be expected, as a result of shallow cumulus overshooting: this is a process which erodes the thickness of the SAL and dries the monsoon layer. Also highlighted in Fig. 10 is the direction of the wind in the monsoon layer that we observed on 28 August 2000. This resembles the thermally direct circulation expected in association with heat-low dynamics, and expected to vary diurnally. In general, we also expect previous rainfall events to influence the nature of the ML and local circulations in the monsoon layer (Taylor *et al.* (2003)) (not shown in schematic).

The SAL above the monsoon layer is characterized by higher θ_v and much lower humidity. Since the isentropes that characterize the SAL connect the Sahara to the zone of deep convection to the south, we can anticipate that the SAL is a region which is efficient for transport of atmospheric constituents between the CBL in the Sahara and the free troposphere at lower latitudes, (since adiabats in the SAL cross the ML top, and the diurnal variability of the ML depth over the Sahara amounts to around 400 hPa). This lateral exchange was evident in the observed humidity structure, which indicated interweaving of moist and dry layers within the SAL. While the humidities in the SAL are generally low, our observations identified a region with high RH at the top of the SAL consistent with a layer of intermittent stratocumulus cloud observed south of 13°N on 28 August and south of 18°N on 29 August. This stratocumulus probably occurs in association with the increase of RH towards the top of a mixed layer, and possibly through detrainment of water vapour from previous convective events originating in the monsoon layer. Such cloud layers are likely to have a big impact on the surface energy budget below, and should be considered in future analyses (and modelling) of the region.

Beneath all of these layers in Fig. 10 we have also highlighted the convective ML. Consistent with the idealized study of the heat-low diurnal cycle of Rácz and Smith (1999), we expect this layer to grow every day into the relatively stable monsoon-layer. To the north, over the Sahara, the ML at the time of our observations (around 1100 UTC) is still relatively shallow. As a result, the SAL is composed of a region above the monsoon layer which is detached from the land surface, and a region to the north which communicates through dry convection with the land surface for some period of the day after sunrise.

Apart from meridional, adiabatic exchanges, which are suggested by the layering of humidity variables, deep cumulonimbus systems traverse the SAL and appear to detrain in the free troposphere. These systems are expected to entrain dry SAL air as they pass through this zone, but are unlikely to detrain significantly in the SAL, since this layer is close to being dry adiabatic. In the free troposphere above the SAL, the atmospheric profile is again close to pseudoadiabatic, with a small baroclinicity which serves to diminish the easterly winds with height. It is intriguing to note that the top of the SAL, where the stability increases with height, occurs close to the 0 °C isotherm. This phenomenon has been observed elsewhere, in environments associated with deep tropical convection (Betts 1986; Johnson *et al.* 1996), and may be associated with the

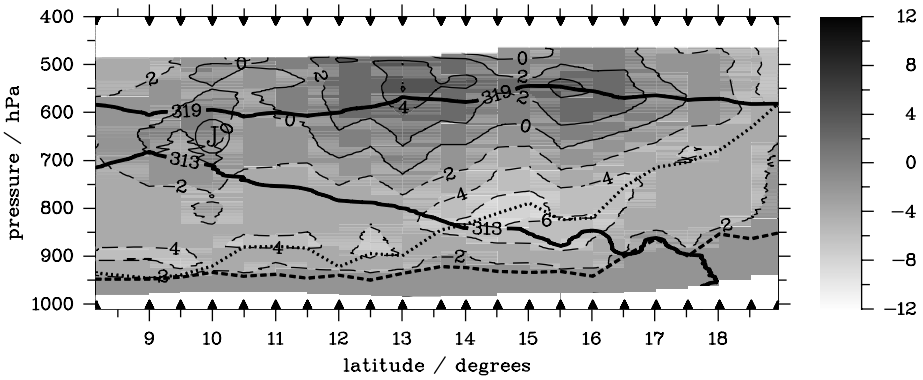

Figure 11. As Fig. 2(b) but for the temperature difference (contoured at 2 K intervals) between air parcels lifted vertically from the mixed layer (ML) in a pseudoadiabatic process and their environment.

melting layer within clouds being communicated into the environment by gravity-wave propagation.

The presence of the SAL above the monsoon layer is expected to have a strong impact on the nature of the resulting moist convection and storms that exist in this region. The near dry adiabatic lapse rate in the SAL provides high conditional instability. The warm base of the SAL will contribute to the convective inhibition (CIN) of parcels in the ML, and the cool upper portions of the SAL contribute to high convective available potential energy (CAPE). Figure 11 shows a plot of parcel buoyancy for air lifted pseudoadiabatically from the ML. Regions of negative buoyancy occur in the upper part of the monsoon layer and the lower SAL, and correspond to CIN. The highest parcel-buoyancies occur at the top of the SAL, in the range of latitudes where the ML θ_e is a maximum, and these buoyancies contribute to the CAPE. Although the magnitudes of the buoyancy features are sensitive to the ML θ_e, which is changing in time as the ML grows, their vertical gradients are approximately fixed by the thermal profile (Parker 2002), and the conditional instability of the SAL means that parcel buoyancy increases rapidly with height in this layer. Thus we expect the intermediate range of latitudes, in which the monsoon layer is overlain by the SAL, to be associated with intense but sporadic deep convection. In addition to the effects of the temperature profile on ascending cloud parcels, low humidity at the base of the SAL will suppress the vertical growth of cumulus, through entrainment (Mapes and Zuidema 1996). The low humidity (and θ_e) of the SAL at mid-levels is also conducive to the generation of evaporatively driven downdraughts and high downdraught CAPE (DCAPE; see Emanuel (1994), p. 172). Since the baroclinic zone has vertical shear, the resulting cold-pool shear interactions can enable long-lived propagating MCSs to develop in the region (e.g. Takeda 1971; Moncrieff and Miller 1976; Houze and Betts 1981; Thorpe *et al.* 1982). Although the magnitude of the vertical shear of the zonal wind (inferred as a vertical gradient from Fig. 2(a)) is roughly constant with latitude at low levels, the bulk wind shear, Δu, between the low-level and mid-level winds is maximized under the AEJ core (see Garner and Thorpe 1992; LeMone and Moncrieff 1994). Interestingly, these conditions of high CAPE, high DCAPE and favourable shear occur poleward of the AEJ. This would suggest that peak MCS activity may occur poleward of the latitudes of peak rainfall.

The schematic presented in Fig. 10 and the concept of these different layers in the baroclinic zone has strong similarities with the models of the AEJ–ITCZ region

shown in previous schematics (e.g. Hamilton and Archbold 1945; Buckle 1996, p. 140; Hastenrath 1991, p. 170 and p. 174). In these previous models, air masses are separated by a sloping 'monsoon trough' or 'intertropical discontinuity' (ITD), which can be related to the line of confluence of the meridional wind (taken to be $v = 0$). In the present study, this is replaced by the base of the SAL, which sits above the sloping baroclinic zone and is defined here by a θ_v surface (marked in bold). Using this adiabatic definition of the interface between the monsoon layer and the SAL is attractive in that it is related to the dynamics and thermodynamics of the AEJ system, through its relation to stability and to lateral transport.

The position of the line of confluence (or $v = 0$) at the surface has been widely used in synoptic analysis, and is often termed the inter-tropical front (ITF). In addition to its dynamic definition, forecasters also use thermodynamic measures to locate the ITF (e.g. Eldridge (1957) recommended the use of a contour of dew point $T_d = 60\,^{\circ}\mathrm{F}$ ($\approx$15 °C) and noted that strong humidity gradients make this measure relatively insensitive to the absolute choice of T_d). We make no claim for the use of an adiabatic contour to denote the ITF, since at low levels it is profoundly affected by diabatic processes in the mixed layer, and since the horizontal gradients of θ_v in the mixed layer can be much weaker than humidity gradients, potentially leading to large errors.

Buckle (1996, p. 140) also indicates a 'wedge' of north-easterlies overriding the monsoon south-westerlies. In Fig. 10, this wedge is replaced by the low-static-stability SAL region that is approximately bounded by the $\theta_v = 313$ K and $\theta_v = 319$ K contours (marked in bold), and is considerably shallower at its lower boundary than the trough line indicated by Buckle (1996). In our synoptic observations, the winds in each layer of the system are more complex than the climatological picture (a characteristic alluded to by Eldridge (1957)). There is considerable vertical shear, and sign-reversals of meridional wind, within the monsoon and SAL regions. In the monsoon layer, the zonal and meridional winds appear to be controlled by boundary-layer and moist-convective processes which act over diurnal and shorter time-scales. In the SAL there are multiple layers of northerly and southerly winds, associated with layering in the thermodynamic tracers. Broadly, during the JET2000 flights there was northerly flow in the lower part of the SAL, but we can expect these patterns to be sensitive to the current phase of AEW activity—recall that on the date shown here, AEW patterns were relatively weak.

The high-resolution data have also enabled us to assess the extent to which the winds are in balance with the observed temperature distribution. Even on these short time-scales, the AEJ is found to be close to geostrophic balance, despite the occurrence of recent deep cumulonimbus systems in the region. Around the region of the jet maximum, the latitude and structure of the AEJ are in good agreement with thermal-wind balance. The vertical shear below the jet, however, is found to be subgeostrophic, implying a tendency for the zonal component of vorticity to increase (implying a thermally direct circulation).

Using dropsonde data from two parallel flight legs, we have performed PV computations for comparison with previous observational estimates and operational analyses. The anticipated PV-structure, with high PV to the south of the AEJ and low PV in the Saharan boundary-layer, is confirmed. The high resolution of these observations gives indications of the low-PV air being advected over the monsoon layer from the Sahara, helping to confirm the Saharan origin of the SAL.

This case serves to remind us that the climatological AEJ arises through a combination of two-dimensional processes (in which the AEJ is set up in approximate geostrophic balance, involving interactions between the heat low and the ITCZ) and weather systems including MCSs and AEWs, that essentially disrupt this picture.

It is important to know more about the two-dimensional processes as well as the impacts and contributions of the more intermittent and three-dimensional weather systems.

In order to take the work forward observationally, there are various recommendations which could be made. Primarily, we have noted that JET2000 took place during a spell of weak AEW activity, and with an AEJ maximum that was some way south of its climatological mean. This was constrained by the operational requirements of the aircraft detachment, which were decided months in advance. In order to ensure aircraft observations of strong AEW structure and different phases of AEJ variability, flights on more days would be required. Secondly, with one aircraft, limited flying hours and limited surface-based observations, it was not possible to make a systematic study of mesoscale and short time-scale patterns, notably the important question of the response of the system to deep convective events. In this regard, additional flights, as well as the provision of an enhanced programme of radiosondes and radar provision for a period before and after flights, would be an enormous advantage. Overall, JET2000 achieved its aims of providing synoptic upper-air data for model validation and diagnostic analysis. It is hoped that future campaigns, such as the internationally planned AMMA experiment, will take this further.

Acknowledgements

JET2000 was funded by NERC grant GR3/13118. We would like to thank our colleagues at the Meteorological Research Flight of the Met Office for the conduct of the aircraft campaign and assistance with data processing. The SCM code for dropsonde analysis was kindly provided by Dr Richard Forbes of the JCMM. Chris Thorncroft has been partially funded for this work by NSF (PTAEO: 1023911-1-24796) and NOAA (1032978-1-28969). We have had many helpful discussions with Dr Chris Taylor, not least in the design and planning of JET2000.

References

Betts, A. K. 1986 A new convective adjustment scheme. Part I: Observational and theoretical basis. *Q. J. R. Meteorol. Soc.*, **112,** 677–691

Bretherton, C. S. and Smolarkiewicz, P. K. 1989 Gravity waves, compensating subsidence and detrainment around cumulus clouds. *J. Atmos. Sci.*, **46,** 740–759

Buckle, C. 1996 *Weather and climate in Africa.* Addison-Wesley Longman, Harlow, UK

Burpee, R. W. 1972 The origin and structure of easterly waves in the lower troposphere of North Africa. *J. Atmos. Sci.*, **29,** 77–90

Caniaux, G., Lafore, J.-P. and Redelsperger, J.-L. 1995 A numerical study of the stratiform region of a fast-moving squall line. 2. Relationship between mass, pressure and momentum fields. *J. Atmos. Sci.*, **52,** 331–352

Carlson, T. N. 1998 *Mid-latitude weather systems*. American Meteorological Society, Boston, MA, USA

Cook, K. H. 1999 Generation of the African easterly jet and its role in determining West African precipitation. *J. Climate*, **12,** 1165–1184

Daley, R. 1995 *Atmospheric Data Analysis*. Cambridge University Press, Cambridge, UK

Diongue, A., Lafore, J.-P., Redelsperger, J.-L. and Roca, R. 2002 Numerical study of a Sahelian synoptic weather system: Initiation and mature stages of convection and its interactions with the large-scale dynamics. *Q. J. R. Meteorol. Soc*., **128,** 1899–1928

Eldridge, R. H. 1957 A synoptic study of West African disturbance lines. *Q. J. R. Meteorol. Soc.*, **83,** 303–314

Eltahir, E. A. B. and Gong, C. L. 1996 The dynamics of wet and dry years in West Africa. *J. Climate*, **9,** 1030–1042

Emanuel, K. A. 1994 *Atmospheric Convection*. Oxford University Press, Oxford, UK

Garner, S. T. and Thorpe, A. J. 1992 The development of organized convection in a simplified squall-line model. *Q. J. R. Meteorol. Soc.*, **118,** 101–124

Hamilton, R. A. and Archbold, J. W. 1945 Meteorology of Nigeria and adjacent territory. *Q. J. R. Meteorol. Soc.*, **71,** 231–264

Hastenrath, S. 1991 *Climate dynamics of the tropics.* Kluwer, Dordrecht, Netherlands

Houze, R. A. and Betts, A. K. 1981 Convection in GATE. *Rev. Geophys. Space Phys.*, **19,** 541–576

Johnson, R. H., Ciesielski, P. E. and Hart, K. A. 1996 Tropical inversions near the 0 degrees C level. *J. Atmos. Sci.*, **53,** 1838–1855

Karyampudi, V. M. and Carlson, T. N. 1988 Analysis and numerical simulations of the Saharan air layer and its effect on easterly wave disturbances. *J. Atmos. Sci.*, **45,** 3102–3136

Karyampudi, V. M., Palm, S. P., Reagen, J. A., Fang, H., Grant, W. B., Hoff, R. M., Moulin, C., Pierce, H. F., Torres, O., Browell, E. V. and Melfi, S. H. 1999 Validation of the Saharan dust plume conceptual model using lidar, Meteosat and ECMWF data. *Bull. Am. Meteorol. Soc.*, **80,** 1045–1075

LeMone, M. A. and Moncrieff, M. W. 1994 Momentum and mass-transport by convection bands—comparisons of highly idealized dynamical models to observations. *J. Atmos. Sci.*, **51,** 281–305

Mapes, B. E. and Zuidema, P. 1996 Radiative–dynamical consequences of dry tongues in the tropical troposphere. *J. Atmos. Sci.*, **53,** 620–638

Matthews, A. J. 2004 Intraseasonal variability over tropical Africa during northern summer. *J. Climate*, **17,** 2427–2440

Moncrieff, M. W. 1992 Organized convective systems: Archetypal dynamic models, mass and momentum flux theory, and parametrization. *Q. J. R. Meteorol. Soc.*, **118,** 819–850

Moncrieff, M. W. and Miller, M. J. 1976 The dynamics and simulation of tropical cumulonimbus and squall lines. *Q. J. R. Meteorol. Soc.*, **102,** 373–394

Newell, R. E. and Kidson, J. W. 1984 African mean wind changes between Sahelian dry and dry periods. *J. Climatol.*, **4,** 27–33

Parker, D. J. 2002 The response of CAPE and CIN to tropospheric thermal variations. *Q. J. R. Meteorol. Soc.*, **128,** 119–130

Parker, D. J. and Burton, R. R. 2002 The two-dimensional response of a tropical jet to propagating lines of convection. *J. Atmos. Sci.*, **59,** 1263–1273

Parsons, D. P., Yoneyama, K. and Redelsperger, J.-L. 2000 The evolution of the tropical western Pacific atmosphere–ocean system following the arrival of a dry intrusion. *Q. J. R. Meteorol. Soc.*, **126,** 517–548

Pedder, M. 1993 Interpolation and filtering of spatial observations using successive corrections and Gaussian filters. *Mon. Weather. Rev.*, **121,** 2289–2902

Pytharoulis, I. and Thorncroft, C. 1999 The low-level structure of African easterly waves in 1995. *Mon. Weather Rev.,* **127,** 2266–2280

Rácz, Z. and Smith, R. K. 1999 The dynamics of heat lows. *Q. J. R. Meteorol. Soc*., **125,** 225–252

Raymond, D. J. and Blyth, A. M. 1992 Extension of the stochastic mixing model to cumulonimbus clouds. *J. Atmos. Sci.*, **49,** 1968–1983

Redelsperger, J.-L., Diongue, A., Diedhiou, A., Ceron, J.-P., Diop, M., Gueremy, J.-F. and Lafore, J.-P. 2002 Multi-scale description of a Sahelian synoptic weather system representative of the West African monsoon. *Q. J. R. Meteorol. Soc.*, **128,** 1229–1257

Reed, R. J., Norquist, D. C. and Recker, E. E. 1977 The structure and properties of African wave disturbances as observed during Phase III of GATE. *Mon. Weather Rev.*, **105,** 317–333

Robe, F. R. and Emanuel, K. A. 2001 The effect of vertical wind shear on radiative–convective equilibrium states. *J. Atmos. Sci.*, **58,** 1427–1445

Schubert, W. E., Ciesielski, P. E., Stevens, D. E. and Kuo, H.-C. 1991 Potential-vorticity modelling of the ITCZ and the Hadley circulation. *J. Atmos. Sci.*, **48,** 1493–1500

Takeda, T. 1971 Numerical simulation of a precipitating convective cloud: The formation of a 'long-lasting' cloud. *J. Atmos. Sci.*, **28,** 350–376

Taylor, C. M., Ellis, R. J., Parker, D. J., Burton, R. R. and Thorncroft, C. D. 2003 Linking boundary-layer variability with convection: A case-study from JET2000. *Q. J. R. Meteorol. Soc.*, **129,** 2233–2254

Thorncroft, C. D. and Blackburn, M. 1999 Maintenance of the African easterly jet. *Q. J. R. Meteorol. Soc.*, **125,** 763–786

Thorncroft, C. D. and Hoskins, B. J. 1994 An idealized study of African easterly waves. Part 1: A linear view. *Q. J. R. Meteorol. Soc.*, **120,** 953–982

Thorncroft, C. D., Parker, D. J., Burton, R. R., Diop, M., Ayers, J. H., Barjat, H., Devereau, S., Diongue, A., Dumelow, R., Kindred, D. R., Price, N. M., Saloum, M., Taylor, C. M. and Tompkins, A. M. 2003 The JET2000 project: Aircraft observations of the African easterly jet and African easterly waves. *Bull. Am. Meteorol. Soc.*, **84,** 337–351

Thorpe, A. J., Miller, M. J. and Moncrieff, M. W. 1982 Two-dimensional convection in non-constant shear: a model of mid-latitude squall lines. *Q. J. R. Meteorol. Soc.*, **108,** 739–762